coexisting in the grid. The results of the third simulation are plotted in Fig. 3(d). Here we see the field over time converge to zero as all waves are now being absorbed by both PMLs. Just as important is that the system remain stable for having both types of PMLs within the space. Simulations were run for 12,000 timesteps at the courant for the implicit code. We ran the simulations for the explicit FDTD code for 16,000 timesteps at .7 of the courant. Both codes yield similar results, however, only the explicit results are plotted. It should be noted, at least in the explicit code, that for this simulation if we set $\sigma_{\max}\Delta t > 5.0$ the KPML becomes unstable, absorbing the short wavelength incident whistler waves but exhibiting growth in long wavelength waves of the same frequency and eventually saturating the entire space. Therefore, in this case the, the KPML breaks down as an absorbing boundary condition and consequently one must be careful in their choice of $\sigma_{\max}\Delta t$. However, for the free space case of Section IV-A, we found the KPML to be stable for all values of $\sigma_{\max}\Delta t$ so it really depends on the medium that the KPML is matching.

V. Summary

We have developed a new PML formulation, referred to as the KPML, which explicitly takes into account information on the k-vector direction of incident waves. The use of the KPML method is necessitated for media when the k-vector and group velocity vector components normal to the PML are antiparallel, in which case the traditional PML algorithms result in the growth of the waves (rather than their attenuation) within the PML region. We applied the KPML method to the specific case of whistler mode waves in a magnetized plasma and quantified its effectiveness with both reflection coefficient calculations as well as demonstrating the stability of the formulation with time domain simulations. The time domain results were obtained using both explicit and implicit schemes. We are currently investigating methods for optimizing the numerical reflection coefficient of the KPML as well as ways to generalize the KPML method for any anistropic medium whose k-vector and group velocity vectors differ.

Acknowledgment

We thank Dr. Tim Bell for useful discussions.

References

[1] J. P. Berenger, "A perfectly matched layer for the absorption of electromagnetic waves," *J. Computational Phys.*, vol. 114, pp. 185–200, 1994.

[2] W. C. Chew and W. H. Weedon, "A 3-D perfectly matched medium fom modified Maxwell's equations with stretched coordinates," *Micro. Opt. Tech. Lett.*, vol. 7, no. 13, pp. 599–604, Sep. 1994.

[3] V. G. Veselago, "Electrodynamics of substances with simultaneous negative values of ϵ and μ," *Sov. Phys. Usp.*, vol. 10, p. 509, 1968.

[4] G. V. Eleftheriades and K. G. Balmain, *Negative-Refraction Metamaterials*. Piscataway/Hoboken, NJ: IEEE Press/Wiley, 2005.

[5] E. Becache, S. Fauqueux, and P. Joly, "Stability of perfectly matched layers, group velocities, and anisotropic waves," *J. Computational Phys.*, vol. 188, pp. 399–433, 2003.

[6] S. A. Cummer, "Perfectly matched layer behavior in negative refractive index materials," *IEEE Antennas Wireless Propag. Lett.*, vol. 44, no. 12, pp. 1630–1639, Dec. 2005.

[7] ——, "A simple, nearly perfectly matched layer for general electromagnetic media," *IEEE Microw. Wireless Compon. Lett.*, vol. 13, no. 3, pp. 128–130, Mar. 2003.

[8] T. W. Chevalier, U. S. Inan, and T. F. Bell, "Numerical simulation of electric dipole antennas in the inner magnetosphere," presented at the URSI/Radio Science Conf., Boulder, CO, 2006, unpublished.

[9] R. A. Helliwell, *Whistlers and Related Ionospheric Phenomena*. Stanford, CA: Stanford Univ. Press, 1965.

[10] R. Gendrin, "Le guidage des whistlers par le champ magnetique," *Planet. Space Sce.*, vol. 5, pp. 274–282, 1961.

[11] M. W. Chevalier and U. S. Inan, "A PML using a convolutional curl operator and a numerical reflection coefficient for general linear media," *IEEE Trans. Antennas Propag.*, vol. 2, no. 7, pp. 1647–1657, Jul. 2004.

[12] J. A. Roden and S. D. Gedney, "Convolutional PML (CPML): an efficient FDTD implementation of the CFS-PML for arbitrary media," *Microwave Opt. Technol. Lett.*, vol. 27, no. 5, pp. 334–339, 2000.

[13] J. H. Lee and D. K. Kalluri, "Three-dimensional FDTD simulation of electromagnetic wave transformation in a dynamic inhomogeneous magnetized plasma," *IEEE Trans. Antennas Propag.*, vol. 47, no. 7, pp. 1146–1151, Sep. 1999.

[14] E. Hairer, S. P. Nørsett, and G. Wanner, *Solving Ordinary Differential Equations I: Nonstiff Problems*. New York: Springer-Verlag, 2000.

[15] ——, *Solving Ordinary Differential Equations II: Stiff and Differential-Algebraic Problems*. New York: Springer-Verlag, 2002.

[16] M. S. Sarto and A. Scarlatti, "Suppression of late-time instabilities in 3-D-FDTD analyses by combining digital filtering techniques and efficient boundary conditions," *IEEE Trans. Magn.*, vol. 37, p. 3273, 2001.

Application of Matrix Pencil to Obtain the Current Modes on Electrically Large Bodies

M. Felipe Cátedra, Fernando Rivas, Carlos Delgado, José M. Gómez, and Lorena Lozano

***Abstract*—The matrix pencil method, in combination with an interpolation using nonuniform rational bi-spline surfaces, is applied for the expansion of the induced currents on complex bodies in terms of current-modes. The approach is useful for solving electrically large problems of radiation or scattering using physical optics with one or more bounces. The techniques presented in this paper can be also useful to improve some rigorous methods.**

***Index Terms*—Electromagnetic analysis, electromagnetic scattering, parameter estimation, physical optics (PO), radar cross sections, spline functions.**

I. Introduction

Recently, several efficient methods have been developed for the rigorous numerical analysis of radiation and scattering of electrically large problems. The multilevel fast multipole algorithm (MLFMA) has improved the efficiency of the methods based on the solution of an integral equation (IE), [1]. This algorithm makes it unnecessary to compute or store the large and dense impedance matrix that appears when the IE is discretized; furthermore the CPU-time required to evaluate the application of the discretized IE operator to a vector is proportional to $N \log N$, where N is the number of samples. When an iterative method is employed to solve the discretized IE, both the CPU-time and the computer memory needed are only proportional to $N \log N$, which is a great improvement on the efficiency of the numerical method. However, N is proportional to the surface size expressed in terms of squared lambda. Typically a sampling rate in the range of 6 to 10 samples per wavelength is needed. Therefore, due to the dependence of N on the

Manuscript received August 27, 2003; revised January 27, 2006. This work was supported in part by the Spanish Department of Education and Science under Project TEC 2004-03187 and in part by the Madrid Community Project S-0505/TIC/0255.

M. F. Cátedra, C. Delgado, J. M. Gómez, and L. Lozano are with the Departamento de Ciencias de la Computación, Universidad de Alcalá, 28806 Alcalá de Henares (Madrid), Spain (e-mail: felipe.catedra@uah.es).

F. Rivas is with the Departamento de Ingeniería Electrónica de Telecomunicación y Automática, EPS de Linares, Universidad de Jaén, Linares E-23700, Spain.

Digital Object Identifier 10.1109/TAP.2006.879214

square of the frequency, huge computer resources are required for analyzing a large structure (e.g., an aircraft) in the microwave range of frequencies, even when using MLFMA. It must be taken into account that MLFMA needs to compute or to store $Nc*N$ method of moments (MoM) matrix elements, where Nc is the average number of subdomains close to a given one for which a rigorous computation (without the FMA approach) of the coupling with this subdomain is required.

With the aim of overcoming this drawback, the asymptotic phase-front extraction (APE) technique was used to obtain and represent the currents on the smooth surfaces of electrically large perfect electric conducting (PEC) bodies of arbitrary geometry [2]. Using this approach each one of the two components of the current vector function is expressed as a finite series of high frequency terms. Each term of those series is defined by the product of a slowly varying amplitude function that defines the component amplitude and an exponential function which takes into account the phase-variation that also varies slowly, [3]–[5]. We will call these terms "current modes." The two functions that define a mode (amplitude and phase functions) extend over large areas of the body surface, so that each component of the current in the entire body surface can be accurately represented with a small number of these pairs of functions. In fact, both slowly-varying functions can be represented and interpolated from a number of samples M, which is considerably smaller than the number of values required in a direct sampling of the current component N, [6]. Another very important feature is that M depends very weakly on the frequency. This means that an expansion of the current component in such terms will greatly reduce the aforementioned drawback of rigorous methods for high frequencies, particularly considering that the field generated by these current functions can be computed very efficiently, with a computational complexity proportional to M [7]. It should be noted that these current modes could greatly improve the efficiency of iterative methods solving extremely large electromagnetic problems, because they avoid the storage of the MLFMA terms and the huge amount of data resulting from the sampling of the current density when 6 to 10 samples per wavelength are employed. On the other hand, the field generated by the current modes is computed faster because only M samples should be considered in both the integral domain (surface where the current is defined) and in the field domain (surface where the field must be found).

In this work it is assumed that the geometry of the bodies under analysis is described by a set of parametric surfaces. In particular each surface will be described by one or more nonuniform rational bi-spline surfaces (NURBS) [8]. It is also assumed that each NURBS is electrically very large, so that its current can be accurately represented by a set of current modes. NURBS are very useful in the analysis of complex structures because they have been included into several international standards and are widely used for the representation and interchange of the geometrical information in many industrial sectors. It is desirable to exploit the NURBS description of a body working directly over it, without the need of a new remeshing of the body geometries.

The purpose of this paper is to describe an efficient procedure for expanding a known real current on a NURBS in terms of current modes. In order to illustrate the technique in this paper, a physical optics (PO) current is used as the known current. More generally, however, the known current could come from an IE solution.

The expansion of the current on a body in terms of current modes has the following advantages apart from the aforementioned efficiency in the current representation and storage.

— It makes possible a fast computation of the near and far-fields [9].

— It provides useful expressions for understanding the current behavior in the body surface, which mechanisms cause them, etc. This understanding can help to predict the current behavior when the working frequency changes in the problem using the frequency scaling properties of the current modes [2] and [5].

It is assumed that the current is known, at least, in a set of sampling points and around these points. The values of the current at those points are the input data for the procedure presented in the paper. The purpose is to obtain the current modes expansion of the current from this data.

An example of the potential applications of the proposed approach could be an improvement of the MLFMA avoiding the computation and storage of the $Nc * N$ matrix elements between close subdomains in the smooth areas of the body under analysis and accelerating the field computation between far smooth surfaces. These surfaces can represent almost all the body area and therefore the storage and CPU-time saving can be very large. In the smooth areas of the body, the field that a current mode creates over the surface where the mode itself is located is a new current mode with the same phase variation that this current mode plus new modes due to the "diffraction" effect in the boundary lines of the surface where the current mode is defined, if these lines are the edges of any sharp wedge. To apply the current modes approach in combination with MLFMA we shall obtain a representation of the field or error functions in terms of modes in each smooth surface at any step of the iterative scheme used in the MLFMA due to the different current modes in other surfaces, or due to the current near the edge discontinuities, and in general any kind of discontinuity. Once the current for a given iteration is expressed in terms of a few modes, one is able to compute efficiently the field re-radiated by these modes in the following step of the iterative approach [7].

This paper is arranged as follows. Section II presents the definition of the problem to be solved and the model of exponential function series, useful to represent the currents locally around the sampling points considered. It is shown that the parameters of the current modes can be found by solving the exponential terms in the model. Results for three scattering cases are presented in Section III . These cases are a simple flat plate illuminated by two sources, a problem with double reflection between curve surfaces, and the representation of the field that a PO current creates over the same surface where it is defined. The results show that the approach presented is fine to find a useful expansion of the current in terms of modes.

II. Definition of Current Modes

The coordinates of an arbitrary point $(\vec{\mathbf{r}}_0)$ on a surface and the values of a current mode on that point are expressed in terms of the parametric coordinates (u, v) of that surface. This means that the parametric domain space where the geometry and the current mode are defined is quite simple in the parametric space; it is a flat square patch with sides of length 1, defined by $0 \leq u \leq 1$ and $0 \leq v \leq 1$. We use five parametric functions for each current mode on a given piece of a surface. Three parametric functions are for the representation of the x, y and z coordinates of the points of that piece of surface itself in terms of parametric coordinates (u, v). The other two parametric functions are for the representation of the amplitude and the phase, respectively, of the mode. We must notice that the current modes are the terms of the two separate series that represent the u- or a v-component the current $\vec{\mathbf{J}}$ on that surface. We shall use different series for each one of the u- or v-current components of $\vec{\mathbf{J}}$ to represent a surface current whose polarization (elliptical in a general case) can change along the surface points.

In order to find the expression of any of these five functions, a set of sampling points is selected on that surface. Fig. 1 shows an example

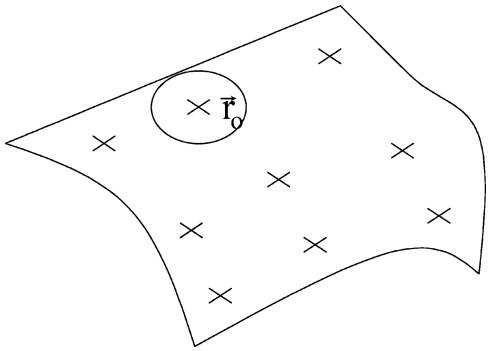

Fig. 1. Example of a surface piece. The sample points where a NURBS patch is interpolated are indicated by crosses.

of a set of sampling points on a piece of the surface of a body. The procedures to obtain the three parametric functions that result in the Cartesian co-ordinates of the points of a surface are well established [8]. Usually, if the direction of the normal vector to the surface piece does not turn more than 30 degrees when we move this vector along all the points of that surface piece, a mesh of 7×7 points contains enough information to interpolate the three parameter functions that represent the geometry of that surface piece as a NURBS. We select the surface pieces following the criterion that the normal vector does not turn more than 30 degrees along the complete surface piece.

Furthermore, as is indicated in [6], the amplitude and phase functions that define a current mode on the surface piece can be obtained as a NURBS using an interpolation from the values of the functions in the sampling points. Considering the accuracy of the interpolation, the phase function is the most critical case. The amplitude function is interpolated using the same number of points and a procedure similar to that used for the three parameters functions that define the Cartesian coordinates. However, it is more complex for the phase function due to a pair of reasons. The first reason is that the acceptable errors are considerable lesser for the phase function than for the Cartesian coordinates or the mode amplitude functions. For instance, an error of 0.1 per cent can be acceptable for the Cartesian coordinates or mode amplitude function, but not for the phase function if this last one varies in a range of thousands of radians. The second reason is that it is not always possible to use a direct procedure as the one indicated in [6], where the phase function of the current mode is interpolated from the "unwrapped phase," because the unwrapped phase values are not always available. The "unwrapped phase" is the phase value without subtracting an integer number of times 2π radians to force the phase to be in the range $(-\pi, +\pi)$ or, in other words, without any jump of 2π radians. One can use the method indicated in [9] to be able to interpolate the phase function. This method, summarized in Appendix A, uses the spatial frequency vector. The components of the spatial frequency vector are the spatial phase derivatives along the tangent vectors to the surface.

Therefore we are able to interpolate the functions that represent a current mode from the values of its amplitude, phase and spatial frequency vector. Now, we will discuss how to obtain those values from the values of the u- and v-components of the total current density $\vec{\mathbf{J}}$ in the sampling points and in the neighborhood of that points. This is equivalent to solve each components of $\vec{\mathbf{J}}$ in terms of modes.

Using the expansion in terms of current modes, the α-component (α represents u or v) of $\vec{\mathbf{J}}$ can be expressed in the neighborhood of any point $\vec{\mathbf{r}}_0$ in the following form:

$$\mathbf{J}_{\boldsymbol{\alpha}}(\vec{\mathbf{r}}_0 + \Delta\vec{\mathbf{r}}) = \sum_{\mathbf{L}=1}^{\Omega_{\boldsymbol{\alpha}}} \mathbf{A}_{\boldsymbol{\alpha}\mathbf{L}}(\vec{\mathbf{r}}_{\mathbf{o}}) \mathrm{e}^{\mathbf{j}\omega_{\boldsymbol{\alpha}\mathbf{L}\mathbf{u}}(\vec{\mathbf{r}}_{\mathbf{o}})\Delta\mathbf{u} + \mathbf{j}\omega_{\boldsymbol{\alpha}\mathbf{L}\mathbf{v}}(\vec{\mathbf{r}}_{\mathbf{o}})\Delta\mathbf{v}} \tag{1}$$

where $\mathbf{A}_{\boldsymbol{\alpha}\mathbf{L}}$ is the amplitude of the Lth current mode and $\omega_{\boldsymbol{\alpha}\mathbf{L}\mathbf{u}}$ and $\omega_{\boldsymbol{\alpha}\mathbf{L}\mathbf{v}}$ are the components of $\vec{\omega}_{\boldsymbol{\alpha}\mathbf{L}}$, the wave vector of that current mode.

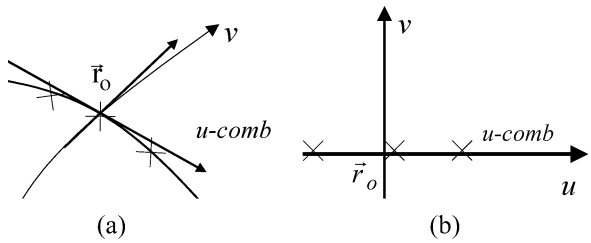

Fig. 2. "u-comb" around a point on the surface: (a) real space and (b) parametric space.

The objective here is to estimate the number of modes (Ω_α), the wave vectors ($\vec{\boldsymbol{\omega}}_{\boldsymbol{\alpha}\mathbf{L}}, L = 1, \ldots \Omega_\alpha$) and the complex amplitudes $\mathbf{A}_{\boldsymbol{\alpha}\mathbf{L}}$ that represent the α-component of the current $\vec{\mathbf{J}}$, at point $\vec{\mathbf{r}}_0$. Once the modes have been solved in the mesh of sampling points used for interpolating in a NURBS, (typically 5×5 or 7×7 sampling points), we can obtain the components of the wave vector for a particular mode in those sampling points and form a continuous function $\vec{\boldsymbol{\omega}}_{\boldsymbol{\alpha}\mathbf{L}}(\mathbf{u}, \mathbf{v})$ using the interpolation procedure indicated in [6]. By repeating the procedure for all the modes of the two components of the current we can obtain the expansion of $\vec{\mathbf{J}}$ in terms of current modes. It must be remarked that we will usually have to deal with a reduced number of modes.

Fig. 2(a) shows the u and v-isoparametric lines which cross the point $\vec{\mathbf{r}}_0$ in a surface. Fig. 2(b) presents the image of that lines in the parametric space defined by u and v. It can be noticed that in the real space the isoparametric lines may be nonorthogonal, as in the example of the figure. Of course, in the parametric space both lines are perfectly orthogonal. In order to extract the u-component of the wave-vector and the amplitude of the current modes (i.e., $\boldsymbol{\omega}_{\boldsymbol{\alpha}\mathbf{L}\mathbf{u}}$ and $\mathbf{A}_{\boldsymbol{\alpha}\mathbf{L}}$ $l = 1, \ldots \Omega_\alpha$; $\alpha = u$ or v), an array of points close to $\vec{\mathbf{r}}_0$ along the u-isoparametric line is selected. Usually, a number ranging from 6 to 16 sampling points in the array is enough. In the example of Fig. 2 these points are indicated by crosses. From now on, we will say that these points belong to the so-called "u-comb" at $\vec{\mathbf{r}}_0$. In the same way, the "v-comb" is defined in a neighborhood of $\vec{\mathbf{r}}_0$. Fig. 2(a) shows that the points constituting the "u-comb" are not exactly on the tangent to the u-isoparametric line, but they are at a negligible distance from that tangent because all of them are all very close to $\vec{\mathbf{r}}_0$.

It is assumed that the α-component of the current $\vec{\mathbf{J}}$ is known for all the points of the "u-comb." Let $\vec{\mathbf{r}}_1$ be a generic point in the "u-comb," and let Δu be the increment in the u-parametric co-ordinate from point $\vec{\mathbf{r}}_0$. The α-component of $\vec{\mathbf{J}}$ at $\vec{\mathbf{r}}_1$ is given by

$$\mathbf{J}_{\boldsymbol{\alpha}}(\vec{\mathbf{r}}_1) = \sum_{\mathbf{L}=1}^{\Omega_{\boldsymbol{\alpha}}} \mathbf{A}_{\boldsymbol{\alpha}\mathbf{L}}(\vec{\mathbf{r}}_{\mathbf{o}}) \mathrm{e}^{\mathbf{j}\omega_{\boldsymbol{\alpha}\mathbf{L}\mathbf{u}}(\vec{\mathbf{r}}_{\mathbf{o}})\Delta\mathbf{u}}. \tag{2}$$

The points of the "u-comb" can be conveniently chosen so that the distance between two consecutive points is uniform. Therefore, it is possible to express $\mathbf{J}_{\boldsymbol{\alpha}}$ for the ith point of the "u-comb" in the following way:

$$\mathbf{J}_{\boldsymbol{\alpha}}(\vec{\mathbf{r}}_{\mathbf{i}}) = \sum_{\mathbf{L}=1}^{\Omega_{\boldsymbol{\alpha}}} \mathbf{A}_{\boldsymbol{\alpha}\mathbf{L}}(\vec{\mathbf{r}}_{\mathbf{o}}) \mathrm{e}^{\mathbf{j}\omega_{\boldsymbol{\alpha}\mathbf{L}\mathbf{u}}(\vec{\mathbf{r}}_{\mathbf{o}})\Delta\xi(\mathbf{i}-1)}. \tag{3}$$

The working hypothesis of the method is that the values $\boldsymbol{A}_{\alpha\boldsymbol{L}}$ and $\boldsymbol{\omega}_{\alpha\boldsymbol{L}\boldsymbol{u}}$ of the αL-mode do not vary along the u-comb points. This hypothesis requires that the electrical length of the u-comb be very small, generally smaller than the wavelength. The parameters defining the current modes in (3), (i.e., the number of modes $-\Omega_{\boldsymbol{\alpha}}$- and their frequencies and amplitudes- $\boldsymbol{A}_{\boldsymbol{\alpha}\boldsymbol{L}}$ and $\boldsymbol{\omega}_{\boldsymbol{\alpha}\mathbf{L}\boldsymbol{u}}$ $\boldsymbol{L} = 1, \ldots \Omega_\alpha$), could be obtained using Fourier spectral estimation, like in [2]. However, if we use a small

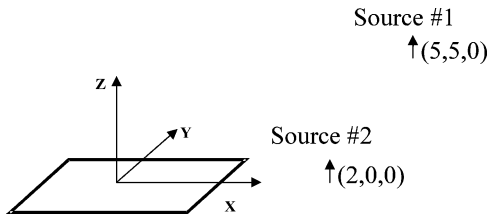

Fig. 3. Geometry of the first case considered to test the approach.

length for the u-comb in order to satisfy the mentioned working hypothesis, the Fourier estimation gives very poor resolution, and if the length of the comb is made larger the hypothesis fails and errors in the estimation can appear. In order to obtain good resolution for the spatial frequency and amplitude of the modes, high resolution methods for spectral estimation [10] should be considered. These methods provide much higher resolution than Fourier-based methods when the length of the "u-and v-combs" is quite limited. From the so-called "super resolution methods," the matrix pencil (MP) method, [11] (see Appendix B), has been chosen, because it is numerically very efficient and it works well with noiseless coherent signals, as in the case of finding the exponential parameters of expression (3). In particular, we have used MP considering the consecutive sampling points of the "u-and v-combs" separated about 0.05 to 0.1 wavelength. The total number of sampling points in each comb, typically a number between 6 and 16, is chosen to be a bit greater than twice the number of expected modes. This size of the combs is a trade off between the need that the working hypothesis be satisfied and the minimum size required by the MP. It should be noticed that MP requires uniformly separated sampling points but works with coherently related signals, as in the case of the estimation of the current modes parameters. Other spectral estimation methods, like for instance MUSIC, [10], can work with nonuniform sampling points, but are not applicable for coherent related modes.

The v-component of the spatial frequency vector, $\boldsymbol{\omega_{\alpha Lv}}$, of the αL-mode, can be obtained considering the v-comb at point $\vec{\mathbf{r}}_0$, see Fig. 3. The expansion of the α-component of the current around $\vec{\mathbf{r}}_0$ is, now, given by

$$\mathbf{J}_\alpha(\vec{\mathbf{r}}_\mathbf{i}) = \sum_{\mathbf{L}=1}^{\Omega_{\boldsymbol{\alpha}}} \mathbf{A}_{\boldsymbol{\alpha}\mathbf{L}}(\vec{\mathbf{r}}_\mathbf{o}) e^{\mathbf{j}\boldsymbol{\omega}_{\boldsymbol{\alpha}\mathbf{L}\mathbf{v}}(\vec{\mathbf{r}}_\mathbf{o})\Delta\xi(\mathbf{i}-1)}. \tag{4}$$

By applying the MP method to (4) we obtain again, in addition to the frequencies $\boldsymbol{\omega_{\alpha Lv}}$, the number of modes $\Omega_{\boldsymbol{\alpha}}$, and the amplitudes $\boldsymbol{A_{\alpha L}}$. The spatial frequency components associated to the same amplitude $\boldsymbol{A_{\alpha L}}$ in the expansion of the α-component of the current along the u and v- combs are paired to obtain the two components of the spatial frequency vector $\vec{\boldsymbol{\omega}}_{\boldsymbol{\alpha}\mathbf{L}}$ at point $\vec{\mathbf{r}}_0$. By interpolating the values of the spatial frequency vector $\vec{\boldsymbol{\omega}}_{\boldsymbol{\alpha}\mathbf{L}}$ from its values in the mesh of sampling points using the method shown in [6], we can obtain the values of the vector function $\vec{\boldsymbol{\omega}}_{\boldsymbol{\alpha}\mathbf{L}}(\mathbf{u},\mathbf{v})$ for all the points of the surface we are studying.

III. Results

The first example to show the performances of the proposed method is a case with a perfect electric conducting square plate of side 1 meter, see Fig. 3. The surface plate is described by only one NURBS. The origin of the coordinate system is located at the center of the plate with the z-axis perpendicular to the plate. The parameter coordinates chosen are such that the u and v-parametric coordinates coincide with the x and y-axis, respectively. Two vertical electric dipoles located at points (5.,5.,0.) and (2.,0.,0.), referred to *Source* # 1 and *Source* #2 , respectively, radiate to the plate. The working frequency is 10 GHz. It has been assumed that the total current induced in the plate is the PO current due to both sources. Obviously, the total PO current due to both dipoles is formed by only four modes, that is two current modes for each current component, u or v. On the other hand each source originates a current mode in the u- or v-component. Although it is a very simple case, it should be noted that the amplitudes and the wave vector components change along the plate surface and therefore it is a full problem of solving and interpolating the current modes from a very small number of samples.

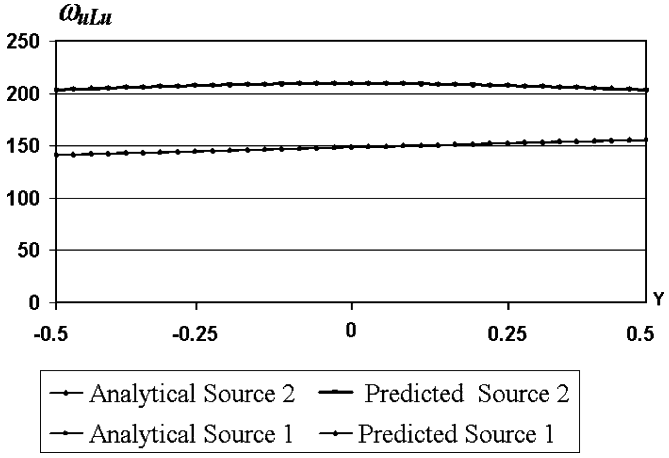

Fig. 4. Predicted values of the u-component of the wave vectors for both modes of the u-component of the current compared with the analytical solution.

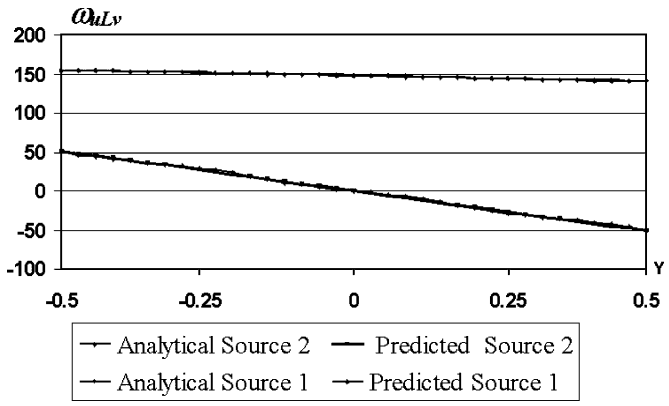

Fig. 5. Predicted values of the v-component of the wave vectors for both modes of the u-component of the current compared with the analytical solution.

In order to detect the current modes, the so-called "u-comb" and "v-comb" have been defined using 8 points, spaced 0.1λ. A mesh of 7 $\times$ 7 pairs of u-combs and v-combs have been used on an array of 7 $\times$ 7 interpolating points. From the values of the current modes in these points and using NURBS themselves for the interpolation, the amplitude functions $\mathbf{J}_{\boldsymbol{u}L}(\boldsymbol{u},\boldsymbol{v})$ and $\mathbf{J}_{\boldsymbol{v}L}(\boldsymbol{u},\boldsymbol{v})$ and the wave-vector components $\boldsymbol{\omega}_{\boldsymbol{\alpha Lu}}(\boldsymbol{u},\boldsymbol{v})$ and $\boldsymbol{\omega}_{\boldsymbol{\alpha Lv}}(\boldsymbol{u},\boldsymbol{v})$ can be obtained over the complete plate.

Figs. 4 and 5 show the cut along the isoparametric line $u = 0$ (y-axis) of the components $\boldsymbol{\omega}_{\boldsymbol{uLu}}(\boldsymbol{u},\boldsymbol{v})$ and $\boldsymbol{\omega}_{\boldsymbol{uLv}}(\boldsymbol{u},\boldsymbol{v})$ of the wave vectors of the two modes, obtained analytically and with the present approach. As expected, the two modes are detected. An excellent agreement between the numerical and analytical values is shown for both functions $\boldsymbol{\omega}_{\boldsymbol{uLu}}(\boldsymbol{u},\boldsymbol{v})$ and $\boldsymbol{\omega}_{\boldsymbol{uLv}}(\boldsymbol{u},\boldsymbol{v})$.

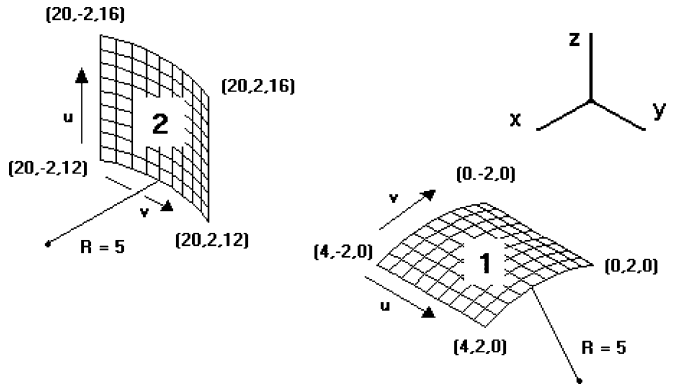

Fig. 6. Test case with two curve surfaces. Each surface is a piece of cylinder with a radius of 5 m. The axis of the cylinder that defines surface 1(2) is parallel to the y-axis (z-axis). The Cartesian co-ordinates of all the vertices are indicated in meters.

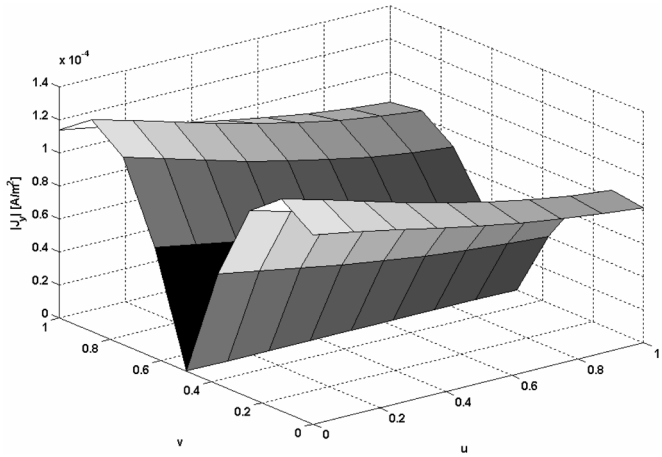

Fig. 8. Amplitude of the y-component of induced current in surface 2 of Fig. 6.

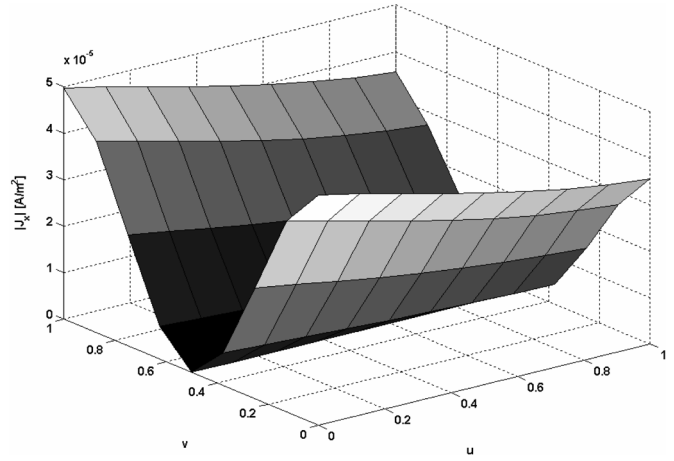

Fig. 7. Amplitude of the x-component of the current mode in surface 2 of Fig. 6.

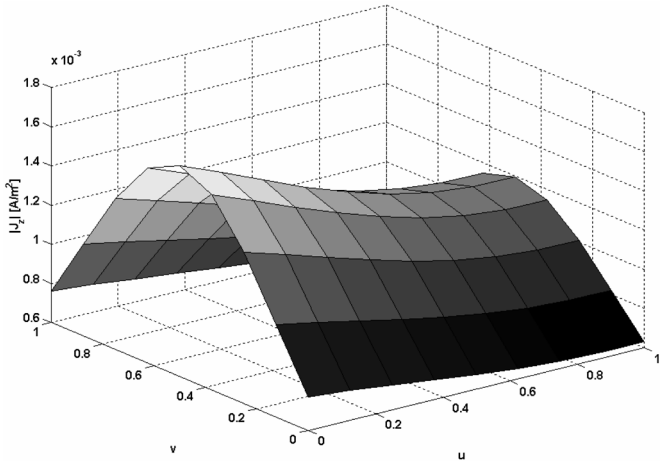

Fig. 9. Amplitude of the z-component of induced current in surface 2 of Fig. 6.

The second case considered is the problem with two curve surfaces whose geometry is indicated in Fig. 6. An incident θ-polarized plane wave is considered in the direction $\phi = 180^\circ, \theta = 45^\circ$. The frequency is 500 MHz. The surfaces sides have a length of 4 m (6.66 wavelengths at the working frequency). In order to analyze the behavior of the current modes approach when the field source is not a point-source we have considered the induced current in surface 2 of Fig. 6 by the PO current of surface 1 due to the incident wave. The current in surface 2 of this second reflection is computed considering, again, the PO approach. Only a current mode per component is obtained using the MP method to extract the current modes of the current in surface 2 due to double reflection. Figs. 7–9 show the amplitude of the Cartesian components of the current due to these modes. A mesh of 7×7 sampling points has been considered to represent these current modes in the NURBS that defines surface 2. The MP has been applied in each one of those sampling points considering arrays of 9 points to define the corresponding u- and v-*combs*. The value of the L parameter in the MP application has been 5 and the electrical length of both combs is 1.4 wavelengths.

In order to evaluate the accuracy of the current modes approach, Fig. 10 shows the error between a pure numerical evaluation of the PO integral and the current mode solution for the z-component of the induced current in surface 2 of Fig. 6. To obtain the error a new mesh of points on surface 2 is considered. The points of the new mesh are located between the points of the mesh of (7×7) sampling points considered to interpolate the current modes. The purely numerical PO is calculated considering the magnetic field at the points of the new mesh due to the PO current of the first reflection in surface 1. The values of the current mode at those points are evaluated using the interpolation technique shown in [6]. We can see that the error of the current mode representation is very small, about 0.001 per cent.

The third case considered is the computation of the electric field that a current mode creates over itself. This is probably the worst case for the current modes approach, since now the computation of near field values is required. The geometry is defined by the cylindrical sector indicated in Fig. 11. It is assumed that the surface supports the current mode that represents the PO current of a simple reflection due to an incident θ-polarized plane wave that arrives in the direction $\phi = 0^\circ$, $\theta = 0^\circ$, with a frequency of 2.0 GHz. The electrical length of the straight sides of the surface is about 13.333 wavelengths and a little greater for the curve sides. The electric field originated by the PO current due to the simple reflection is expanded in terms of modes ("electrical field modes," in this case). Three field modes have been detected using the MP method for the x-polarization. A picture of the amplitudes of two of these modes is shown in Figs. 12 and 13. As in case 2, a mesh of 7×7 sampling points has been considered to represent the modes and the MP has been applied with the same parameter values: arrays of 9 points to define the corresponding u- and v-*combs*, L parameter fixed to 5 and the electrical lengths of both combs of 1.4 wavelengths. Fig. 14 presents the relative error between a purely numerical evaluation of the electrical field, and the addition of the three field modes detected in a mesh of points located between the mesh of (7×7) sampling points

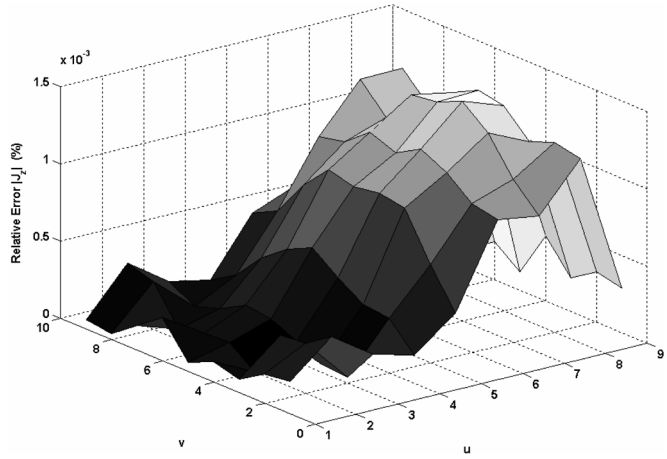

Fig. 10. Values of the relative error for the z-component of induced current in surface 2 of Fig. 6.

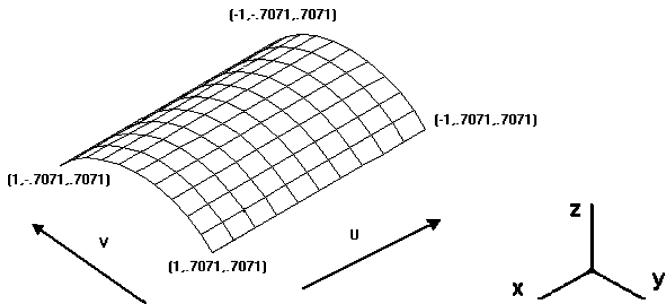

Fig. 11. Test case geometry for the study of the modes in a "self-induced" field. The surface is a 90° sector of a cylindrical surface with a radius of 1.0 m. The cylinder axis is located in the x-axis. The Cartesian co-ordinates of the four vertices are indicated in meters.

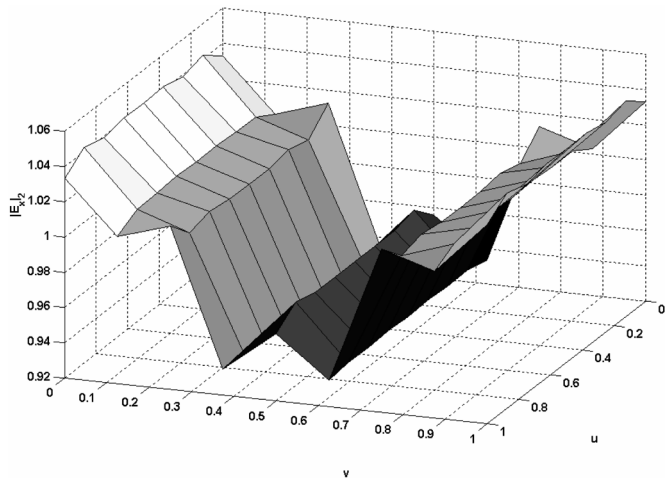

Fig. 12. Amplitude of the x-component of the field mode 1.

used for interpolating the current modes by the same procedure that in case 2. Now again, we can see that the field modes represent with acceptable accuracy the electrical field even for the difficult computation of the self-induced field.

IV. Conclusions

An approach has been developed to solve the current modes of a surface current from its values at a small number of sampling points. The

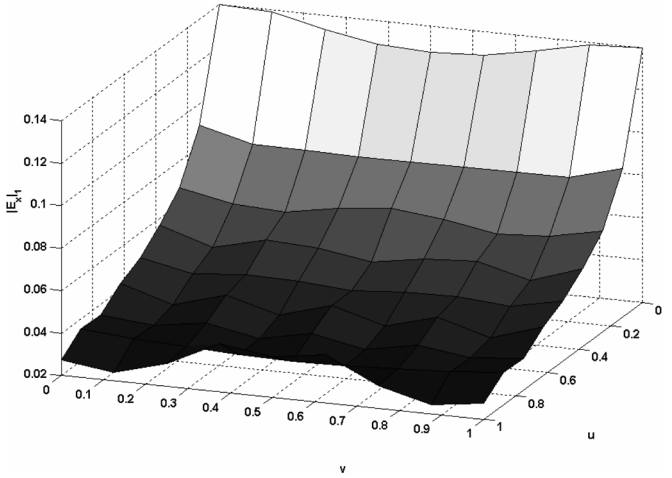

Fig. 13. Amplitude of the x-component of the field mode 2.

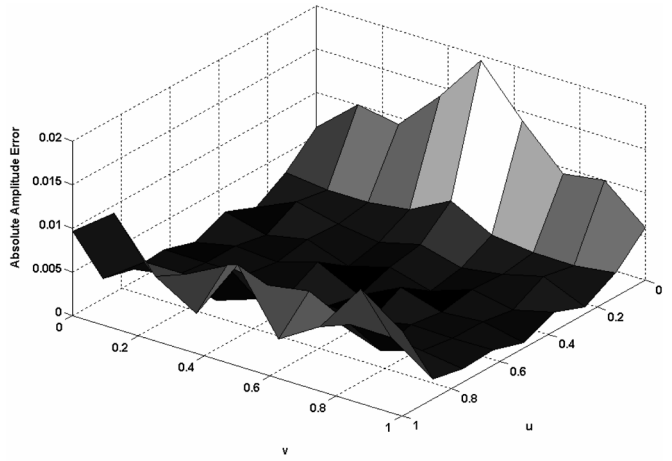

Fig. 14. Amplitude of the error of the total x-component of the field.

approach can be very useful when the surface currents can be expressed as a few current modes, because in this case they can be represented using a small amount of data, much lesser than using an expansion of the current in terms of subdomain functions. This feature of the current appears many times in the surfaces of smooth curvature in high frequency problems. The approach can be directly applied to the analysis of high frequency problems using a PO approach with multiple bounces. As shown in [7], [9] and [12] the PO integrals of multiple bounce problems can be computed very efficiently using quasi-analytical expressions when the current is expanded in terms of current modes. The approach could be applied also to solve rigorously electrically large problems using iterative methods provided that in many surfaces of the problem the solution (the current) can be expressed in terms of a few modes. In these cases the computations of the mutual coupling between surface parts required in the iterative process can be accelerated also using the approach shown in [7], [9] and [12].

Appendix A
Current Mode Interpolation

We assume that the amplitude $\mathbf{J_o}(\mathbf{u},\mathbf{v})$ and the spatial frequency components $\boldsymbol{\omega_u}(\mathbf{u},\mathbf{v})$ and $\boldsymbol{\omega_v}(\mathbf{u},\mathbf{v})$ of a current mode are functions that vary smoothly in the surface where the current mode is defined. These functions can be obtained in the surface piece where the mode is defined by interpolation from their values in the sampling points. This

interpolation can be performed using different approaches, for instance in terms of new NURBS as described in [6].

The phase function $\mathbf{\Phi}(\mathbf{u},\mathbf{v})$ of the mode will be obtained considering that the components of its gradient are the spatial frequencies of the current mode

$$\nabla\mathbf{\Phi} = \frac{\partial\mathbf{\Phi}}{\partial\mathbf{u}}\hat{\mathbf{u}} + \frac{\partial\mathbf{\Phi}}{\partial\mathbf{v}}\hat{\mathbf{v}} = \boldsymbol{\omega}_{\mathbf{u}}\hat{\mathbf{u}} + \boldsymbol{\omega}_{\mathbf{v}}\hat{\mathbf{v}}. \tag{a.1}$$

After the interpolation the spatial frequency components $\boldsymbol{\omega}_{\mathbf{u}}(\mathbf{u},\mathbf{v})$ and $\boldsymbol{\omega}_{\mathbf{v}}(\mathbf{u},\mathbf{v})$ are expressed in terms of polynomial expansions. Therefore, analytical expressions for the phase can be obtained by integrating the spatial frequency components. We will denote by $\mathbf{\Phi}_{\mathbf{u}}$ and $\mathbf{\Phi}_{\mathbf{v}}$ the analytical expressions obtained by integrating the u and v frequency components, respectively

$$\mathbf{\Phi}_{\mathbf{u}}(\mathbf{u},\mathbf{v}) = \int \boldsymbol{\omega}_{\mathbf{u}}(\mathbf{u},\mathbf{v})\mathbf{du} \tag{a.2.a}$$

$$\mathbf{\Phi}_{\mathbf{v}}(\mathbf{u},\mathbf{v}) = \int \boldsymbol{\omega}_{\mathbf{v}}(\mathbf{u},\mathbf{v})\mathbf{dv}. \tag{a.2.b}$$

Ideally, the analytical functions $\mathbf{\Phi}_{\mathbf{u}}$ and $\mathbf{\Phi}_{\mathbf{v}}$ should differ only in a constant value along the surface points. An averaged phase function can be obtained from

$$\mathbf{\Phi}_{\mathbf{m}}(\mathbf{u},\mathbf{v}) = \left(\mathbf{\Phi}_{\mathbf{u}}(\mathbf{u},\mathbf{v}) + \mathbf{\Phi}_{\mathbf{v}}(\mathbf{u},\mathbf{v})\right)/\mathbf{2}. \tag{a.3}$$

Now, an accurate expression for a phase function, useful for a rectangular subregion around the sampling point $(\mathbf{u_o},\mathbf{v_o})$, is obtained using the averaged phase function $\mathbf{\Phi_m}$

$$\Phi_{\mathrm{o}}(\mathrm{u},\mathrm{v}) = \Phi_{\mathrm{m}}(\mathrm{u},\mathrm{v}) + \Phi(\mathrm{u_o},\mathrm{v_o}) - \Phi_{\mathrm{m}}(\mathrm{u_o},\mathrm{v_o}) \tag{a.4}$$

where $\Phi(\mathrm{u_o},\mathrm{v_o})$ is the value of the phase at the sampling point.

The size of the rectangles around the sampling points are chosen in such a way that they form a tessellation that covers completely the surface piece where the current mode is defined and each sampling point corresponds with a rectangle center.

Appendix B
Matrix Pencil Method

Matrix Pencil (MP) Method estimates the frequencies from exponentially damped or undamped sinusoidal data sequences. To introduce the MP Method let us assume we have undamped sinusoidal sequences in the following uniform sequence:

$$\mathrm{x_i} = \sum_{\mathrm{l}=1}^{\mathrm{M}} |\mathrm{h_l}| \mathrm{e}^{(\mathrm{j}\omega_{\mathrm{l}}(\mathrm{i}-1)+\Phi_{\mathrm{l}})} \tag{b.1}$$

where $\mathrm{i} = 0, 1, \ldots \mathrm{N}-1$.

In our case x_i represents the $\mathrm{J}_u(u,v)$ or $\mathrm{J}_v(u,v)$ components of the field at the i-sampling point of an u or v comb and $w_l(i-1)$ corresponds to $(\omega_{\mathrm{lu}}(\vec{\mathrm{r}}_{\mathrm{o}})\Delta\mathrm{u})$ or $(\omega_{\mathrm{l_v}}(\vec{\mathrm{r}}_{\mathrm{o}})\Delta\mathrm{v})$ in (1).

Sequence (b.1) may be rewritten as

$$x_i = \sum_{l=1}^{M} h_l z_l^{(i-1)} \tag{b.2}$$

with

$$h_l = |h_l| e^{j\Phi_l} \tag{b.3}$$

and

$$\mathrm{z_l} = \mathrm{e}^{(\mathrm{j}\omega_{\mathrm{l}})}. \tag{b.4}$$

MP Method estimates the M complex frequencies which appear in (b.2). To do that the sequence is arranged in the following way in order to define two matrices G_1 and G_2:

$$[G_1]_{(N-L)xL} = \begin{bmatrix} \mathrm{x_1} & \mathrm{x_2} & \cdots & \mathrm{x_L} \\ \mathrm{x_2} & \mathrm{x_3} & \cdots & \mathrm{x_{L+1}} \\ \vdots & \vdots & & \vdots \\ \mathrm{x_{N-L}} & \mathrm{x_{N-L+1}} & \cdots & \mathrm{x_{N-1}} \end{bmatrix} \tag{b.5}$$

$$[G_2]_{(N-L)xL} = \begin{bmatrix} \mathrm{x_2} & \mathrm{x_3} & \cdots & \mathrm{x_{L+1}} \\ \mathrm{x_3} & \mathrm{x_4} & \cdots & \mathrm{x_{L+2}} \\ \vdots & \vdots & & \vdots \\ \mathrm{x_{N-L+1}} & \mathrm{x_{N-L+2}} & \cdots & \mathrm{x_N} \end{bmatrix}. \tag{b.6}$$

The parameter L (pencil parameter) should be such that $M \le L \le N$. In our calculations, L is assumed to be 2/3N.

Once the matrices G1 and G2 have been defined, the generalized eigenvalues of the following problem are calculated:

$$(\mathrm{G}_2 - \xi\mathrm{G}_1)\mathrm{p} = 0 \tag{b.7}$$

If $M \le L \le N$, this generalized eigenvalue problem gives rise to M main eigenvalues and $(M-N)$ minor eigenvalues, roughly null. Therefore, the number of principal eigenvalues of (b.7) coincides with the number M of frequencies, w_l, to determine. The frequencies w_l are obtained from $\xi_i = z_i$ where $i = 1, \cdots, M$

It is easy to identify the number M of exponential terms in (b.1). This is due to the fact that (b.7) gives rise to N eigenvalues, from which, M of them have a significant value (that is why these eigenvalues are called principal eigenvalues) and the rest of eigenvalues, $M-N$, are roughly zero (these eigenvalues are called ninor eigenvalues). The gap between the last principal eigenvalue and the largest ninor eigenvalue depends on the signal to noise ratio (SNR) of the data. This gap is very large for high value of the SNR. In our case the data in (b.1) are the field values in the sampling points u or v combs, that are noiseless data, (except for the negligible noise introduced by the truncation error due to the finite number of bits used to represent numbers), so we have an extremely large SNR and therefore it is easy to identify the principal eigenvalues from the cutoff defined by the gap between eingenvalues.

Once that the exponential terms in (b.1) have been determined and taking into account (b.2), (b.3) and (b.4) the following equations system can be formulated:

$$\begin{bmatrix} x_1 \\ x_2 \\ \vdots \\ x_N \end{bmatrix} = \begin{bmatrix} z_1^0 & z_2^0 & \cdots & z_M^0 \\ z_1^1 & z_2^1 & \cdots & z_M^1 \\ & & \ddots & \\ z_1^{(N-1)} & z_2^{(N-1)} & \cdots & z_M^{(N-1)} \end{bmatrix} \begin{bmatrix} h_1 \\ h_2 \\ \vdots \\ h_M \end{bmatrix}. \tag{b.8}$$

That can be expressed more compactly as

$$\mathbf{X} = \mathbf{ZH} \tag{b.9}$$

with

$$\mathbf{X} = \begin{bmatrix} x_1 \\ x_2 \\ \vdots \\ x_N \end{bmatrix}; \quad \mathbf{Z} = \begin{bmatrix} z_1^0 & z_2^0 & \cdots & z_M^0 \\ z_1^1 & z_2^1 & \cdots & z_M^1 \\ & & \ddots & \\ z_1^{(N-1)} & z_2^{(N-1)} & \cdots & z_M^{(N-1)} \end{bmatrix}$$

$$\mathbf{H} = \begin{bmatrix} h_1 \\ h_2 \\ \vdots \\ h_M \end{bmatrix}. \tag{b.10}$$

To determine the amplitudes h_l of the exponential terms in (b.1), (the modes in our electromagnetic problem) (b.9) is multiplied by the pseudo inverse matrix of $\mathbf{Z}$ (referred as $\mathbf{Z}^T$).

$$\mathbf{Z}^T\mathbf{X} = \mathbf{H} \tag{b.11}$$

REFERENCES

[1] W. C. Chew, J. Jin, E. Michielssen, and J. Song, Eds., *Fast and Efficient Algorithms in Computational Electromagnetics*. New York: Artech House, 2001.

[2] D.-H. Kwon, R. J. Burkholder, and P. H. Pathak, "Efficient method of moments formulation for large PEC scattering problems using asymptotic phasefront extraction (APE)," *IEEE Trans. Antennas Propag.*, vol. AP-49, pp. 583–590, Apr. 2001.

[3] K. R. Aberegg and A. F. Peterson, "Application of the integral equation phase method to two-dimensional scattering," *IEEE Trans. Antennas Propag.*, vol. AP-43, pp. 534–537, May 1995.

[4] Z. Altman, R. Mittra, O. Hashimoto, and E. Michielssen, "Effective representation of induced currents on large scatterers using the generalized pencil of functions method," *IEEE Trans. Antennas Propag.*, vol. AP-44, pp. 57–57, Jan. 1996.

[5] Z. Altman and R. Mittra, "A technique for extrapolating numerically rigorous solutions of electromagnetic scattering problems to higher frequencies and their scaling properties," *IEEE Trans. Antennas Propag.*, vol. AP-47, pp. 744–751, Apr. 1999.

[6] O. Gutierrez, F. Saez de Adana, F. Rivas, I. Gonzalez, and M. F. Cátedra, "Method to interpolate the induced current with a low amount of sample points by means of Bézier surfaces," *Electron. Lett.*, vol. El-39, pp. 177–178, Jan. 2003.

[7] M. F. Cátedra, C. Delgado, S. Luceri, and F. Saez de Adana, "Efficient procedure for computing fields created by current modes," *Electron. Lett.*, vol. El-39, pp. 763–764, May 2003.

[8] G. E. Farin, "Curves and surfaces for computer aided geometric design," in *A Practical Guide*, 2nd ed. London, U.K.: Academic Press, 1990.

[9] M. F. Cátedra, C. Delgado, S. Luceri, O. Gutiérrez, and F. Saez de Adana, "Physical optics analysis of multiple interactions in large scatters using current modes," *IEEE Trans. Antennas Propag.*, to be published.

[10] C. W. Therrien, *Discrete Random Signals and Statistical Signal Processing*. New York: Prentice Hall, 1992.

[11] Y. Hua and T. K. Sarkar, "Matrix Pencil Method for estimating parameters of exponentially damped/undamped sinusoid in noise," *IEEE Trans. Acoustic Speech Signal Processing*, vol. ASSP-38, pp. 834–844, May 1990.

[12] C. Delgado, F. Cátedra, O. Gutierrez, I. González, and F. Sáez, "Application of current modes to the analysis of arbitrarily shaped targets using PO with multiple bounces," in *Proc. ICEAA '05, Int. Conf. Electromagnetics in Advanced Applications and EESC '05 Eur. Electromagnetic Structures Conf.*, Torino, Italy, Sep. 2005, pp. 1061–1064.

Radar Cross-Section Measurements of a Full-Scale Aircraft Duct/Engine Structure

S. K. Wong, E. Riseborough, G. Duff, and K. K. Chan

***Abstract*—Cavity radar cross-section (RCS) data are measured from a full-sized generic aircraft duct/engine mock-up experimental apparatus. Details of the experimental measurements and characterization of the RCS from a generic aircraft engine inlet with a fan assembly embedded inside are described. The experimental results reveal that the azimuthal RCS patterns from an aircraft engine inlet with fan components embedded inside are very complex.**

***Index Terms*—Cavity radar cross-section, jet-engine inlets, radar cross-section measurements, radar cross-section prediction codes.**

I. INTRODUCTION

A recent research effort in noncooperative target recognition within the Combat ID community involves the development of a synthetic target signature database for target classifiers. For various technical reasons, a synthetically generated database is regarded as the most practical way of fielding an operational target classifier system [1]. Synthetic target signatures are computed using high-frequency electromagnetic radar cross-section (RCS) prediction codes. There has been a great deal of research activities in recent years focusing on cavity RCS modelling of aircraft duct/engine interface. It is known that the inlets of aircraft can produce a significant contribution to the overall RCS of an aircraft. Therefore, cavity RCS computation should be an integral part of the synthetic signature modelling process of aircraft.

In order for any numerical modelling results to be deemed as credible and reliable, they must be validated by experimental data. Although there are many in-depth cavity RCS modelling efforts being conducted in the cavity RCS community [2], [3], there is still a lack of readily available experimental data to validate the numerical analyses. Measured data are scarce in the open literature. A few scale-model and small-sized cavity measurements can be found, for example, Crabtree *et al.* [4] on a straight cylinder with straight blades [0.3 m (diameter) by 0.3 m (length)], Baldensperger *et al.* [5] on an s-bend "Cobra" cavity [0.09 m by 0.11 m (cross section) by 0.35 m (length)], and Odendaal *et al.* [6] on a small unmanned aerial vehicle engine inlet system [0.12 m by 0.36 m (cross section) by 1.0 m (length)]. However, subscale inlet model data have been found to be unreliable as a predictor of full-scale results [7]. For practical aircraft inlet RCS modelling, full-scale experimental data are therefore desirable and pertinent. But there is virtually no experimental data of a full-size duct/engine model available in the open literature. To overcome the shortage of measured data, we have designed and built a generic full-size aircraft duct/engine mock-up for collecting cavity RCS data. The measured data will add to a limited collection of inlet RCS database available in the open literature. This will allow researchers who are working on developing numerical RCS models to have access to some much-needed additional data to validate their works. This communication provides a detailed description of the full-sized duct/engine RCS measurements. A brief summary on the present state of the cavity RCS modelling development is also given.

Manuscript received January 11, 2006; revised April 10, 2006.

S. K. Wong, E. Riseborough, and G. Duff are with the Defence R&D Canada—Ottawa, Ottawa, ON K1A 0Z4, Canada.

K. K. Chan is with the Chan Technologies Inc., Brampton, ON L6Y 5H1, Canada.

Digital Object Identifier 10.1109/TAP.2006.879223